



OPEN

Dielectric breakdown of 2D muscovite mica

Anirudh Maruvada¹, Kalya Shubhakar¹, Nagarajan Raghavan¹, Kin Leong Pey¹ & Sean J. O'Shea²✉

Localized electrical breakdown (BD) measurements are performed on 2D muscovite mica flakes of ~ 2 to 15 nm thickness using Conduction Atomic Force Microscopy (CAFM). To obtain robust BD data by CAFM, the probed locations are spaced sufficiently far apart (> 1 μm) to avoid mutual interference and the maximum current is set to a low value (< 1 nA) to ensure severe damage does not occur to the sample. The analyses reveals that 2D muscovite mica has high electrical breakdown strength (12 MV/cm or more) and low leakage current, comparable to 2D hexagonal boron nitride (h-BN) of similar thickness. However, a significant difference compared to h-BN is the very low current necessary to avoid catastrophic damage during the BD event, even for very thin (2–3 nm) flakes. Further, for mica the BD transient always appear to be very abrupt, and no progressive BD process was definitively observed. These marked differences between mica and h-BN are attributed to the poor thermal conductivity of mica.

The two key drivers of the semiconductor industry are high-performance computing devices and high-density memory devices. Both applications heavily rely on the field-effect transistor (FET) which plays a key role in processing information in the case of computing devices and storing logic in the case of memory devices. The FET requires an ultra-thin insulating material, called the gate dielectric, across which electric fields are applied to tune the current flow in the transistor. At present amorphous oxides such as SiO₂ and HfO₂ commonly serve as the gate dielectric but limitations in the performance of these materials is being encountered as the FET dimensions are scaled down to optimize device performance¹. As a consequence, considerable research has recently focused on using 2D materials as an alternative FET technology² to enable continued miniaturization and long-term performance gains. In addition, there are growing new applications for 2D electronic materials in the fields of neuromorphic computing, quantum devices and photonic integrated circuits³.

An essential material required for a 2D FET is a compatible 2D insulator, which must have high dielectric constant and large effective insulator thickness. To date, hexagonal boron nitride (h-BN) has been considered almost exclusively for use as the 2D insulator⁴. An alternative but far less studied candidate material is 2D mica⁵. Mica is a van-der-Waals mineral whose individual layers can be exfoliated to form a defect-free, atomically flat surface^{6,7}. Several properties potentially make mica an excellent candidate for a 2D insulator, namely its wide band gap with a direct band gap of 5.09 eV⁸, moderately high dielectric constant of 9.4⁹, and high thermal and chemical stability¹⁰.

Mica has been used as an insulating substrate for various heterogeneous 2D material structures, including mica/MoS₂, mica/graphene, mica/graphene oxide, and mica/topological insulator configurations^{11–20}. Of particular interest is the utility of mica in 2D microelectronic devices, and in this regard several recent studies have used mica as an active material in a resistive random memory (RRAM) device²¹ and as the gate insulator in a field effect transistor (FET)^{12,13,17–19}. In all these microelectronic technologies, understanding the dielectric breakdown (BD) of the insulator material is critical to the reliability of the logic or data storage device. However, the BD mechanism of 2D mica has received little attention. Previous studies have been limited to mica ≥ 20 nm thick^{22,23}, and there is only a single graph showing BD data on a 9 nm thick 2D mica sample¹³.

In this work, we investigate the dielectric breakdown of thin 2D mica flakes by local electrical stressing using conduction atomic force microscopy (CAFM). The results are compared with other 2D materials, namely synthetic mica and 2D hexagonal boron nitride (h-BN), to assess its candidacy as a prospective 2D insulator. We find that although the leakage current is low for both muscovite and synthetic mica, comparable to that of h-BN, breakdown occurs at very low current levels (~ 1 nA or less) even for 2–3 layer mica flakes. In comparison, current levels of ~ 100 nA or more are observed for the breakdown of h-BN and we attribute this contrast to the marked difference in thermal conductivity of the two materials.

¹Engineering Product Development, Singapore University of Technology and Design, 8 Somapah Road, Singapore 487372, Singapore. ²Institute of Materials Research and Engineering, Agency for Science Technology and Research, 2 Fusionopolis Way, Singapore 138634, Singapore. ✉email: s-oshea@imre.a-star.edu.sg

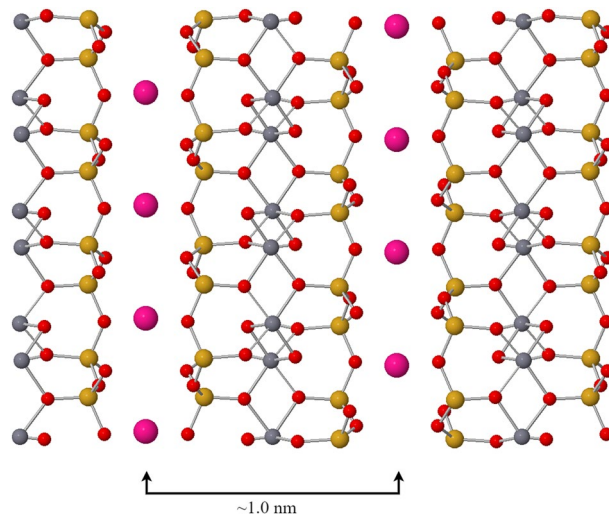


Figure 1. Model of the crystal structure of muscovite mica. The elements are colour coded Red = Oxygen, Grey = Aluminium, Pink = Potassium and Yellow = Silicon. Each mica sheet consists of an aluminium octahedron layer (aluminium, oxygen, hydrogen) sandwiched between two tetrahedron layers (silicon, aluminium, oxygen). Three sheets of mica are shown and potassium ions intercalate in-between these sheets. The mica cleaves readily between the potassium ion planes yielding a step height on exfoliation of 1.0 nm. The model is generated based on the reported literature²⁴.

Before describing the experiments, a brief summary of the mica structure is appropriate. The most commonly studied mica is muscovite mica ($\text{KAl}_2(\text{Si}_3\text{AlO}_{10})(\text{OH})_2$), a naturally occurring material, whose crystal structure consists of an aluminium octahedron sandwiched between two silicon tetrahedron, as shown in Fig. 1²⁴. The silicon tetrahedron layer has a partial substitution of silicon with aluminium to give it a negative charge^{24,25}. Due to this, the positively charged potassium ions (K^+) reside between the mica sheets to compensate for the charge. The mica sheets are held together by van der Waals forces, with one layer being around 1 nm thick, and can be exfoliated using different methods to form clean atomically flat 2D surfaces^{6,7,26}. There are other types of natural mica with differing metal atoms (Fe, Ti, etc.) in the atomic structure. However, for application purposes, synthetic (or fluorophlogopite) mica appears more promising because it is more stable and can be heated to $\sim 1100^\circ\text{C}$ with no degradation as compared to $\sim 550^\circ\text{C}$ for natural mica variants²⁷. Synthetic mica has a similar structure to natural muscovite mica ($\text{KMg}_3\text{AlSi}_3\text{O}_{10}\text{F}_2$) but the hydroxyl group is replaced by a fluoro group. Note that in our work, all the data presented is taken on muscovite natural mica, with the exception of one set of experiments undertaken on Fluorophlogopite synthetic mica shown in Supplementary Fig. S5.

Results

Experimental considerations when measuring 2D mica breakdown. We use gold assisted mechanical exfoliation of mica, as shown in Supplementary Fig. S1, to obtain thin ($< 15\text{ nm}$) and large ($> 4 \times 4\ \mu\text{m}^2$) mica flakes on a gold substrate^{28–30}. CAFM is used to perform localized breakdown (BD) on the flakes by ramp voltage stress (RVS). In RVS, a voltage is linearly applied across the sample at a specific ramp rate until a defined current value (also called compliance current) is reached, at which time, the voltage is turned off to avoid further current injection into the sample. In our setup (shown in Fig. 2), a Keithley 4200 Semiconductor Characterization System is used to force voltage onto the tip and measure the current passing through the tip. The CAFM method operates with a conducting AFM tip in contact with the surface and enables localized BD and current-voltage (I - V) measurements to be made at any location on the surface. In our work, two types of conducting AFM tips are used, namely Platinum Iridium wire cantilevers and conducting diamond cantilevers, with the results being identical for both cantilever types.

The thickness of the transferred mica flakes and local topography (both before and after electrical stressing) are characterized by tapping mode AFM. The production of large flakes is a feature of using the roller transfer method and AFM images show that many of the transferred flakes can be over $10\ \mu\text{m}$ in size (Fig. 3b) with well-defined terraces providing extensive regions of constant thickness over which electrical measurements are undertaken. Thinner regions are often observed near the edge of the larger flakes, as shown in Fig. 3a. In this work, the thickness values over which measurements are taken range from 1.5 to 14 nm i.e., about 1ML to 14ML, where 1ML represents 1 mica layer.

An important aspect of the electrical stress procedure is that two types of RVS are used, as shown in Fig. 4. In one procedure, the voltage is ramped up to a compliance limit with no restraint on the voltage (Fig. 4a). We refer to this as the *standard* approach. However, this method may lead to catastrophic damage to the mica and moreover the behavior of the current leading to breakdown (or equivalently, the charge injection) often cannot be adequately monitored because the current abruptly jumps from a negligibly small value to the current compliance i.e., the current spike at BD can mask small changes occurring just before BD. To monitor charge injection in the electrical breakdown process, we need to control and limit the current spike. We do so by ramping but

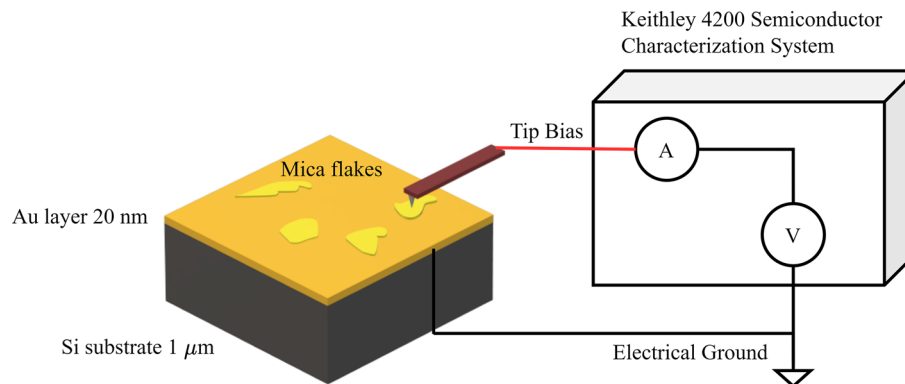


Figure 2. Schematic of the CAFM Setup. Mica flakes exfoliated on a Au substrate which acts as an electrode along with the AFM conducting tip. The electrodes are connected to the Keithley 4200 Semiconductor Characterization System with the substrate grounded.

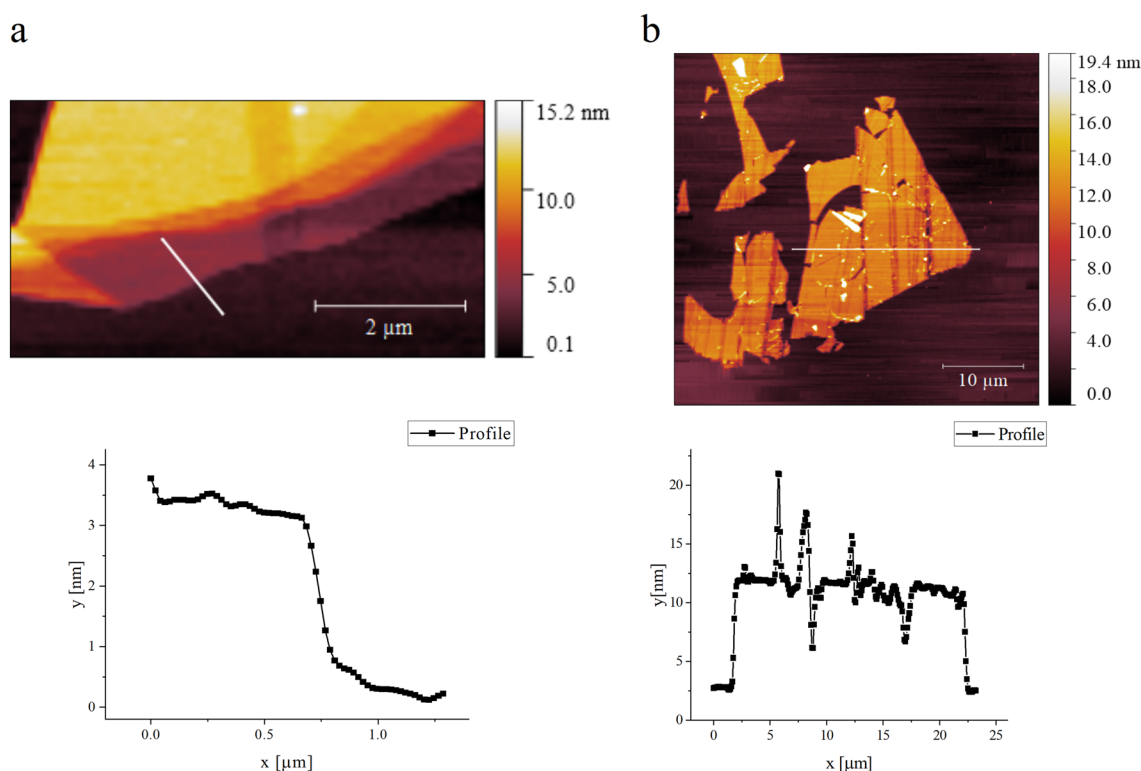


Figure 3. AFM topography images of muscovite mica on Au/Ti/Si substrate. (a) Tapping mode image for a 2–3 nm thick mica sheet with a thickness profile taken along the line indicated shown in the plot below. (b) Tapping mode image for a 9 nm thick mica sheet with a thickness profile taken along the line indicated shown in the plot below.

then stopping the voltage slightly before the BD voltage (V_{BD}), as shown in Fig. 4b. We call this the *voltage limit* approach, and it allows the mica to be continuously stressed prior to breakdown. In the example of Fig. 4b, the first seven cycles show a progressive increase in leakage current on successive stress cycles. At the 8th cycle, an abrupt change in current occurs which is associated with a BD in the material and subsequent cycles (5th and 6th) show considerably lower resistance as expected. The breakdown event itself is quite similar to that measured using the standard approach (Fig. 4a), although V_{BD} is a little smaller and the current change at BD is slightly more gradual rather than an abrupt current spike. Note that V_{BD} is defined at the current spike when the compliance limit is reached e.g., in Fig. 4a $V_{BD} = 8.3$ V at a compliance of 100 pA.

We have found that there are three experimental issues to consider in obtaining consistent CAFM breakdown data, namely (A) an adequate distance between measurement locations must be maintained, (B) swelling of the mica under BD should be kept to a minimum, and (C) a low current compliance limit (~ 100 pA) must be set.

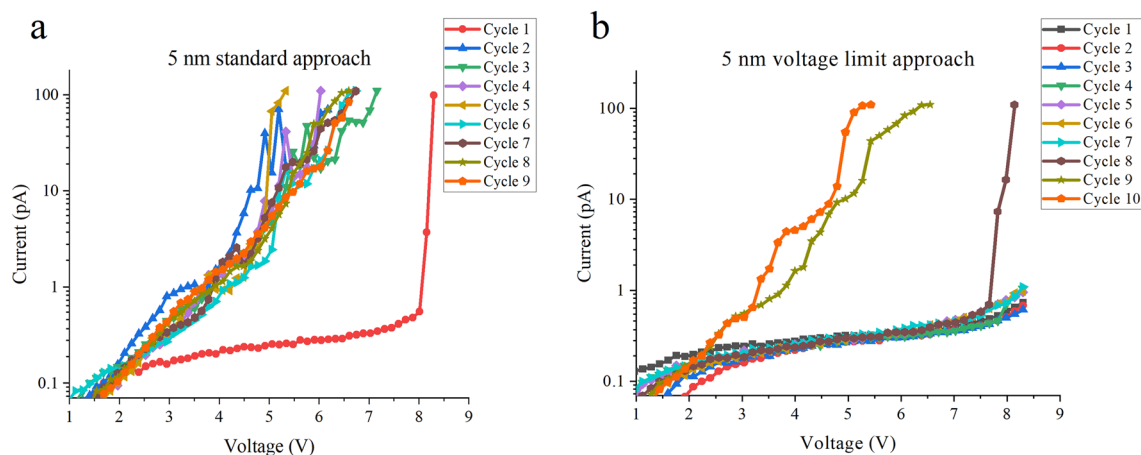


Figure 4. *I-V* curves for 5 nm flakes showing the two types of RVS measurement techniques. (a) Standard RVS with the voltage ramping until the current compliance (100 pA) is reached. (b) Voltage Limit RVS in which the voltage is ramped to slightly below the known BD value, in this case 8.3 V, allowing successive *I-V* to be undertaken before a breakdown occurs. A diamond cantilever is used for both data sets.

These issues are summarized in Fig. 5. Figure 5a shows an AFM image of a pristine 12 nm flake indicating the locations for subsequent BD experiments. Figure 5b shows the same flake after the BD experiments using standard RVS. In this example, structural damage has occurred at all locations except points labelled 4 and 7. However, the associated BD *I-V* curves (Fig. 5c) indicate the breakdown measurement is consistent at all locations. The exception is point 8 which has a much lower V_{BD} and inspection of Fig. 5b shows that this measurement was undertaken between two previous BD experiments (points 0 and 1) which exhibited very extensive damage to the mica. These experiments indicate that for reliable data, measurements must be taken far enough apart (of order $\sim 1 \mu\text{m}$) so as not to influence any subsequent *I-V*. This requirement was also found for h-BN³¹, although the necessary separation was found to be smaller ($\sim 300 \text{ nm}$).

Swelling refers to the observation that after BD, a *hillock* forms at the BD location, as shown by the circled regions of Fig. 5d. The swelling only occurs if a current flows, although it is important to note that the current can be very low with swelling observed even at $\sim 100 \text{ pA}$. Swelling has also been observed in h-BN but at significantly higher current level ($\sim 10\text{--}100 \text{ nA}$)^{31,32}. The origins of the swelling in mica are still not known. Our conjecture is that the swelling is associated with the movement of intercalated potassium ions (K^+) present in muscovite mica under the applied electric field²¹. However, dedicated experiments are needed in future to understand this phenomenon in-depth. From an experimental viewpoint, the *I-V* corresponding to the first BD should be reliable but subsequent *I-V* cycles should be treated with caution if excessive swelling is observed.

Breakdown data on 2D mica. A key finding of our work is that the compliance current must be kept very low ($\sim 100 \text{ pA}$ or less) for CAFM measurements on mica, both to prevent material damage and to allow the charge injection process to be monitored. We observe that increasing the current beyond $\sim 100 \text{ pA}$ typically leads to catastrophic damage of the material, even for very thin films (Supplementary Fig. S2). Obviously, one cannot obtain meaningful data on the post-breakdown characteristics (i.e., measure a 2nd BD *I-V*) over such damaged regions. For comparison, in CAFM experiments undertaken on similar thickness h-BN flakes, much higher currents can be reached before breakdown (see Supplementary Fig. S3), allowing the progressive degradation of the material to be readily observed under repeated RVS stressing at current limits up to $\sim 100 \text{ nA}$ ³¹.

Another major difference compared to h-BN is the breakdown event is very abrupt in mica when standard RVS stressing is used, as shown in Fig. 6a and b. Here, representative breakdown curves for different locations on various mica flakes are plotted and the curves show only minor variability for a given flake thickness. A key feature of all the *I-V* is that the leakage current is very low and the breakdown occurs abruptly. The leakage current through the mica flakes is less than $\sim 1 \text{ pA}$ at 3 V for all thicknesses measured (representing a current density of $\sim 1 \text{ A cm}^{-2}$ or less assuming a typical AFM tip-sample contact area of $\sim 10 \times 10 \text{ nm}^{233}$), even for 1–2 layers, indicating the good insulating properties of this 2D material. For comparison, the approximate thickness corresponding to a leakage current of 1 A cm^{-2} at 1 V bias is 1.7 nm for SiO_2 ³⁴ and 1 nm for exfoliated h-BN³⁵. There is a measurable increase in the current observed prior to BD as charge is injected into the mica, but the onset of the breakdown event itself is very abrupt. The effect of this small current flow is more readily observed in the repeated stressing of a single location using voltage limited RVS, as shown in Fig. 6c and d. In both figures, one observes current flow in Cycle 1, but no breakdown occurs. In Cycle 2, BD occurs, and subsequent *I-V* cycles show a degradation of the dielectric properties of the mica (i.e., lower resistance) under repeated stressing. The BD event is still abrupt but is measured at a slightly lower voltage than that using standard RVS stressing. Clearly charge injection is involved in the BD mechanism, as discussed in more detail below.

Interestingly, we observe the same breakdown trends even for very thin films, as shown in Fig. 7 for a 1–2 nm thick flake which we assign as being 2 layers ($\text{ML}=2$). (Note: For very thin flakes, it is difficult to clearly define the thickness because of the roughness of the underlying gold). The BD is abrupt under standard RVS stressing (Fig. 7a) but shows a progressive degradation under voltage limited RVS with leakage current flow prior to

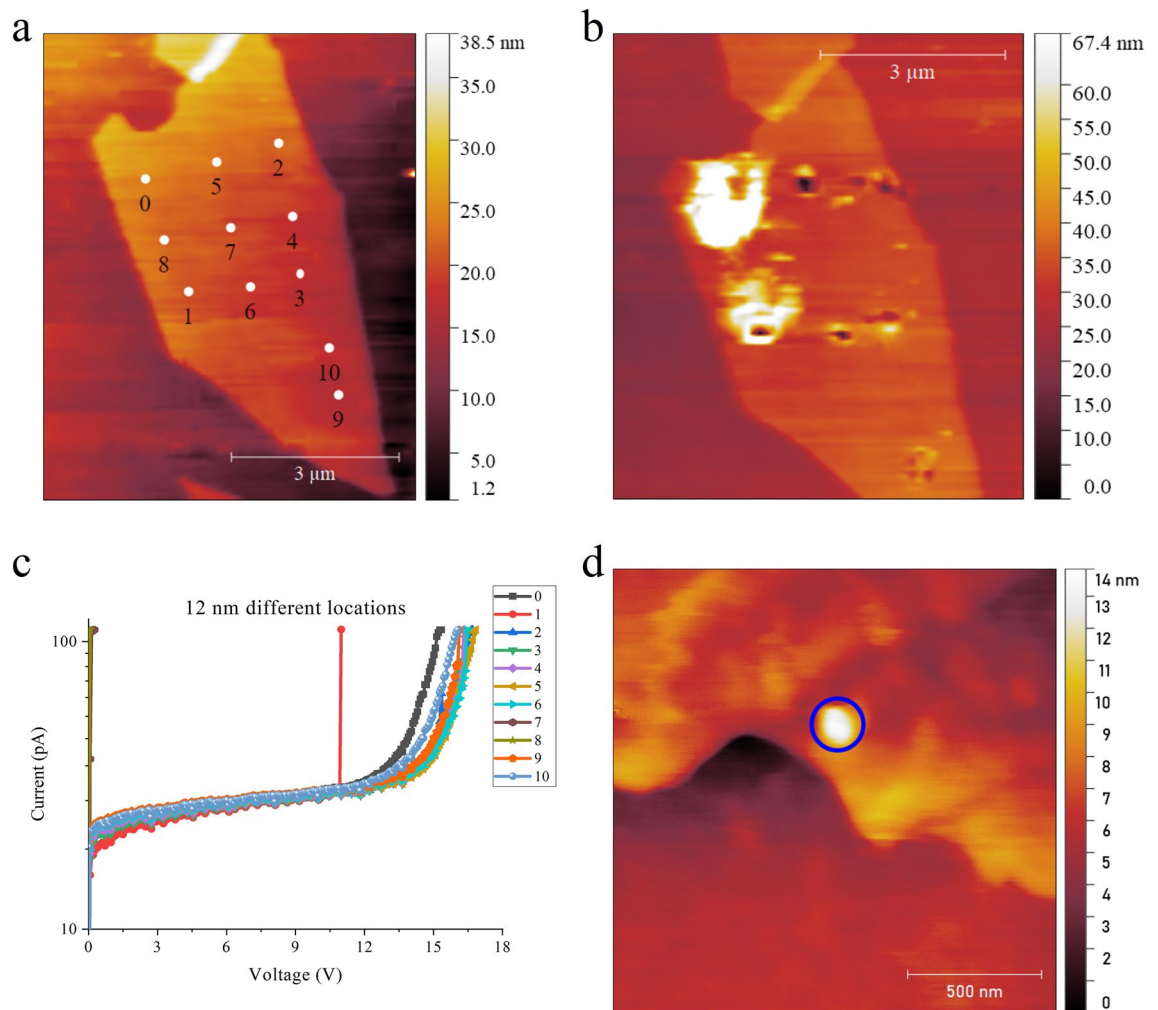


Figure 5. Experimental issues for CAFM measurement of mica dielectric breakdown. **(a)** Topography of a 12 nm mica flake before BD measurements. **(b)** Topography image of the flake after BD measurements using standard RVS with 100 pA compliance. Material damage (pitting) has occurred at the BD locations in this experiment, with the exception of locations 4 and 7. **(c)** The corresponding I - V curves taken during BD show that even though damage occurs, the post-BD locations are far enough apart as to not influence the measurement. The exception is location 8 which is between two large damage areas of Location 0 and 1. A PtIr cantilever is used. **(d)** Swelling (shown circled) on a 5 nm flake after a BD measurement using standard RVS with 100 pA compliance. The swelling is 8 nm in height.

the BD event (Fig. 7b). Subsequently, structural defects such as swelling may be observed at the BD location as shown in Fig. 7c and d. Irreversible damage can also occur if the current compliance is higher than ~ 100 pA (Supplementary Fig. S2). As above, these results indicate that increased current flow prior to BD is integral to the BD mechanism. In this regard, if repeated RVS stressing is undertaken to 1 V below the V_{BD} , then no significant increase in current flow is observed and no BD event occurs.

The average V_{BD} for a given flake thickness can be found by measuring many I - V under standard RVS stressing e.g., I - V as in Fig. 6a and b. The electrical breakdown field strength (E_{BD}) is then found as $E_{BD} = V_{BD}/t_{mica}$ where t_{mica} is the thickness of the flake. The average V_{BD} and E_{BD} values for flakes of different thicknesses is plotted in Fig. 8. It is apparent that the breakdown field is high, comparable to 2D h-BN³¹, and increases as the mica thickness decreases. This follows the same qualitative trend seen for amorphous dielectrics like SiO₂^{36,37}, the 2D dielectric h-BN³¹, and was also noted for thick (> 20 L) mica films²². Possible reasons for the thickness dependence include an increase in local electric fields for thicker layers due to an added contribution from material polarization^{36,37}. Another possible reason could be an increase in the intrinsic defect density of thicker flakes.

Discussion

Comparison with previous experiments. There are only a few related studies reported for thin 2D mica^{13,21,27,38} using either muscovite mica or synthetic mica. The early work of Davidson and Yoffe^{22,23} studied BD in several natural micas and synthetic mica, although the samples tested were much thicker (> 20 ML) than recent studies. Importantly, they find both the BD and conductivity to depend on the type of mica investigated e.g., micas containing Fe and Ti have much higher conductivity. The more recent reports on ultra-thin mica

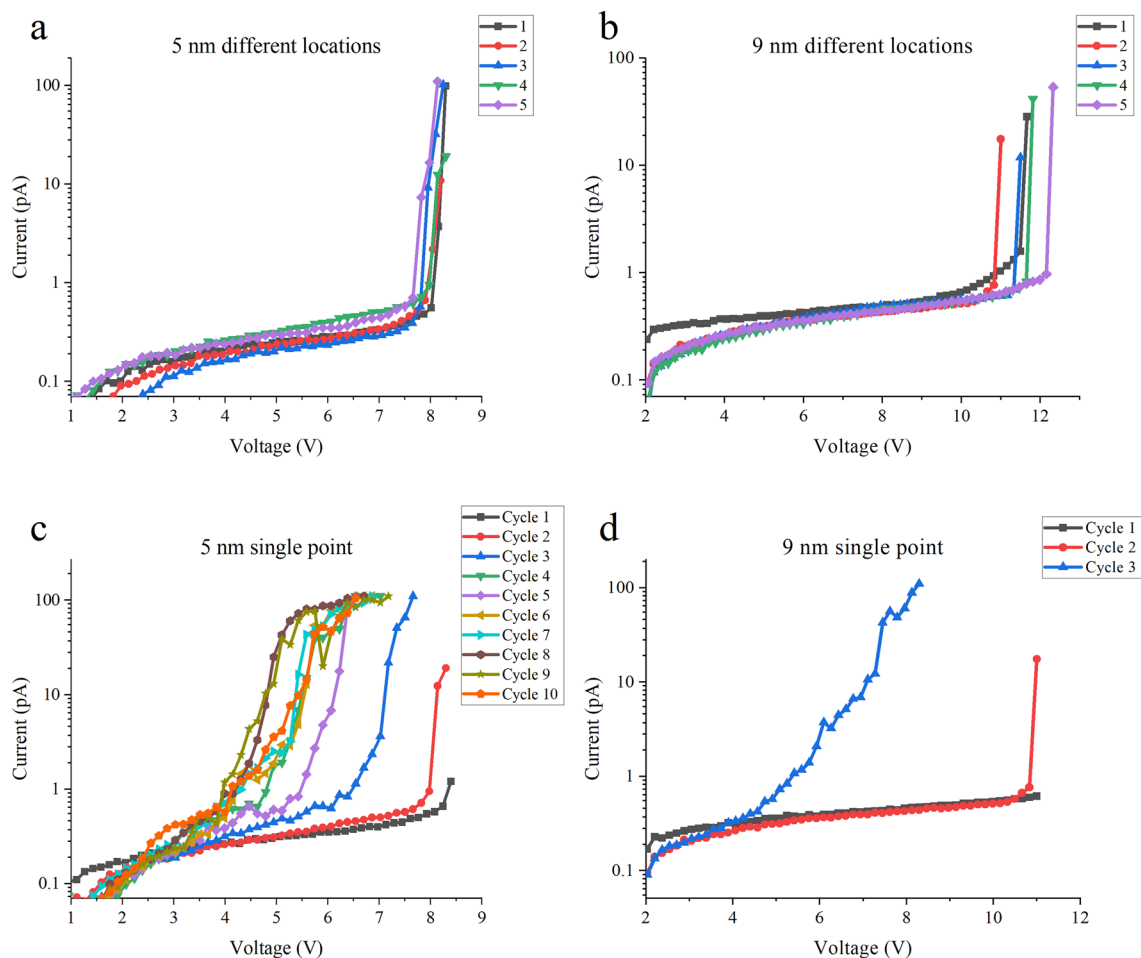


Figure 6. Typical breakdown I - V . BD measured by standard RVS across different points on (a) a 5 nm flake and (b) a 9 nm flake. There is only a small variation of V_{BD} . Repeated stressing by voltage limited RVS measured at a single location on (c) 5 nm and (d) 9 nm flakes. Diamond cantilevers are used for all data.

investigate either muscovite or synthetic mica. Zou et al. studied the BD characteristics using a metal–insulator–semiconductor test capacitor, with 9 nm thick muscovite mica as the insulator layer¹³. A very abrupt BD is observed, just as in our work here, but the reported V_{BD} is lower (~ 8 V) compared to our measurement of $V_{BD} \sim 11$ V on 9 nm flakes. However, Davidson and Yoffe note that capacitor test structures yield noticeably lower V_{BD} than the comparable data taken with a gold metal wire probe²³, because there are more inherent defects in the larger capacitor structure leading to higher currents at a given voltage compared to CAFM.

CAFM studies have also been reported on synthetic mica (Phlogopite mica)²⁷ and muscovite mica³⁸ with the I - V data presented showing currents up to 1 nA and 100 nA, respectively. In our work, we cannot reach these current levels without BD or damage to the mica. Their voltage range is correspondingly also much lower than the voltages in our experiments e.g., for I - V measured on 3ML thickness mica, the current reaches 1 nA at just 3–4 V²⁷ compared to $V_{BD} \approx 5$ –6 V in our work. The difference could be due to the use of different samples given the sensitivity of mica conductivity to mineral content²³, or alternatively the structural difference between dioctahedral (muscovite) versus trioctahedral (phlogopite) i.e., trioctahedral silicate sheets have 3 divalent cations compared to 2 trivalent cations for dioctahedral silicate sheets. We suggest an alternative possibility, namely the mica has undergone breakdown. Neither of the studies^{27,38} mentioned if the data shown represents the first I - V or a subsequent I - V . The I - V reported could therefore reflect the conductivity of the material after BD. Note that the I - V after BD still appears non-linear (Supplementary Fig. S4) but the current for a given voltage is much higher.

The CAFM studies using 2D synthetic mica (Fluorophlogopite mica) as the active material in an RRAM device²¹ provide further support to our observations. Here, a forming voltage is applied across the mica over many RVS cycles to achieve a stable RRAM response. This use of forming voltage is entirely similar to our data taken with a voltage limit RVS. If one carefully considers the I - V data shown for the forming voltage cycles, one can discern that the first I - V is similar to our BD data with the following voltage cycles showing decreasing resistance until the stable RRAM configuration is reached.

Breakdown characteristics of 2D mica. The primary insulating material considered for 2D applications is h-BN and hence it is worthwhile to compare the mica and h-BN breakdown characteristics. The leakage current values measured by CAFM are quite similar (< 1 pA over comparable thickness and measurement ranges)

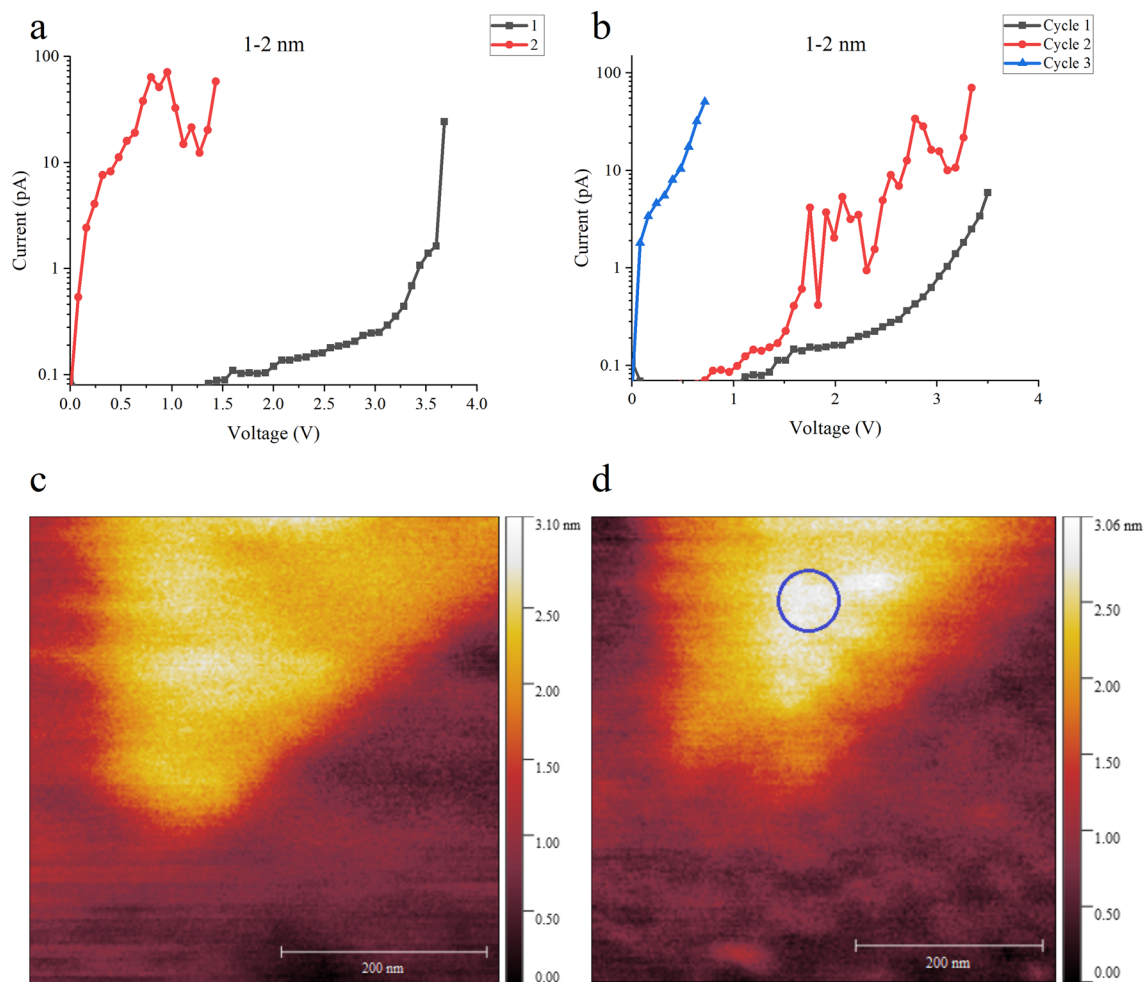


Figure 7. Breakdown data on very thin (1–2 nm) mica flakes, showing similar characteristics as for the thicker films. (a) BD experiment using standard RVS with 100 pA compliance, indicating $V_{BD} = 3.6$ V. A diamond cantilever is used. (b) BD experiment using voltage limit RVS up to 3.5 V with 100 pA compliance, indicating a progressive degradation stage in the BD process. A diamond cantilever is used. Topography of the BD region (c) before and (d) after the BD measurement showing a slight swelling (circled) at the BD location. The swelling is 0.8 nm high.

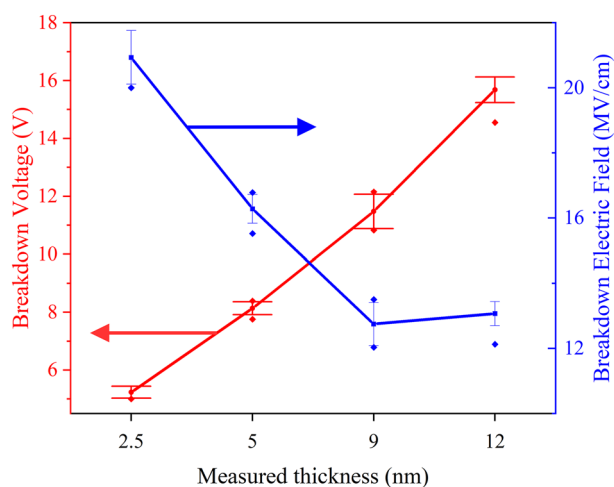


Figure 8. Plot showing the thickness dependence of V_{BD} and E_{BD} , with the solid lines provided as a guide to the eye. The error bars indicate the spread of values measured with different tips and on different flakes.

for both mica and h-BN³⁹ and E_{BD} increases as the film thickness decreases for both materials³¹. A significant difference is the abrupt, catastrophic breakdown for mica at very low currents (< 1 nA), whereas the BD in h-BN occurs at much higher current compliance (> 100 nA) and a progressive layer-by-layer degradation of the dielectric is measured^{31,40,41}, as shown in Supplementary Fig. S3. Catastrophic BD was observed even for 3ML mica films.

This stark contrast in BD behavior between mica and h-BN implies there must be a fundamental difference in the BD energetics. However, an understanding of the BD mechanism at the atomic scale is lacking with further experimental and computational studies required. For example, studies on synthetic mica have shown that intercalated potassium ions under an electric field migrate vertically through the mica layers²¹. In our work, *swelling* resulting from the BD measurement is observed at the tip location and we surmise this arises from the electric field driven movement of K^+ ions. Importantly, swelling only occurs if a relatively significant leakage current is detected *just* prior to BD, suggesting the movements of K^+ ions *may be* significant only during the BD transient. However, the nature or even existence of a BD mechanism involving K^+ remains unknown.

Hence, we limit the discussion to a phenomenological description based on the large body of work available for conventional thin film oxides⁴² and 2D materials⁴³. Broadly, we describe why the BD only occurs at very low current levels and why the BD always appears abrupt and hence, progressive degradation is not observed.

In a conventional gate dielectric such as SiO_2 or HfO_2 , there is an initial wear out phase, followed by the onset of BD in which a current carrying leakage path linking the two electrodes is formed i.e., a percolation path⁴². In our work, a small rise in current is observed in the wear out phase prior to BD and as in other dielectrics, this charge injection gives rise to an accumulation of defects leading to the BD itself^{23,42}. We find charge injection occurs prior to BD for both muscovite mica and synthetic mica (Supplementary Fig. S5). In contrast, whilst Davidson and Yoffe also find current flow prior to BD for natural micas^{22,23}, they observe no measurable current for synthetic mica. We attribute this difference to the much thinner films used in our work. No discrete or digital fluctuations in the current can be observed, but this is to be expected given the very low current levels that must be measured with a correspondingly small measurement bandwidth (~ 1.2 Hz).

The wear out and BD are followed by a third phase in which material damage occurs as rapid changes in power dissipation and local temperature enhancement around the percolation path take place at the BD location. It is the time evolution of this third phase which dictates the experimental observations for mica. Specifically, it has been shown that after the percolation path is formed, the rate of change of the breakdown current (dI_{BD}/dt) is a key parameter in the BD evolution⁴². For thick films (> 10 nm), which necessarily also corresponds to high voltages, the BD transient dI_{BD}/dt is large. Consequently, for SiO_2 and HfO_2 , the BD evolves extremely rapidly (at nanosecond time scales) and when measured using typical instrumentation at the millisecond time scale, always appears as a hard abrupt breakdown. As the film thickness is reduced, and thereby also the corresponding voltage, the kinetics of the BD evolution slows down drastically such that a gradual growth in current may be observed. This is termed progressive BD in SiO_2 and HfO_2 (see Supplementary Fig. S3) which occurs not only because the stress voltage is less but also because the injected electron energy is smaller such that specific breakdown processes cannot be activated⁴². In fact, it has been argued that a progressive BD will always occur in a material, but often the effect is masked as the experimental measurement latency is too slow to catch up⁴². For SiO_2 , the BD transient and related kinetics can be associated with the critical defect density necessary for breakdown (N_{BD}), and the dependence of N_{BD} with SiO_2 thickness is well known⁴⁴. For example, the larger N_{BD} of thick films results in abrupt, fast BD because the large number of defects present near the percolation path means that current can flow along many available paths linking the two electrodes⁴³. Further study needs to be done to verify if this phenomenon also applies to mica.

In our experiments on mica, hard BD is invariably observed, even for very thin films (2ML) at low voltage, indicating dI_{BD}/dt is high and the BD is very fast. Any progressive (i.e., slower) BD features are masked, although there are traces of progressive breakdown in some of the measurements on thinner samples under voltage limited RVS e.g., Figs. 6c and 7b. However, these should be considered only as tentative indicators and further investigation, specifically time-dependent-dielectric-breakdown (TDDDB) experiments, are required. The most likely reason dI_{BD}/dt is always high stems from the poor thermal conductivity of mica ($k_{th} \sim 1$ $Wm^{-1} K^{-1}$). For comparison, 2D h-BN has $k_{th} \geq 100$ $Wm^{-1} K^{-1}$ ⁴⁵. Once a percolation path has formed and more current begins to flow through the BD location, the power generated at the BD increases substantially. In low thermal conductivity materials, the heat cannot be efficiently dissipated and, aided by thermal runaway, the BD spot can rapidly reach very high temperature (> 1000 °C)⁴³ leading to structural damage. The poor heat dissipation also implies that once a BD path has formed, only a very low current is required to initiate thermally induced damage. This appears to be the case for mica because catastrophic BD damage occurs even at ~ 1 nA current compliance as measured by CAFM. Note that a direct comparison of thermal BD effects between mica and conventional gate oxides, which also have poor thermal conductivity (e.g. $k_{th} \approx 1$ $Wm^{-1} K^{-1}$ for SiO_2 ⁴⁶), is complicated by the fundamental structural difference between the materials i.e. SiO_2 and HfO_2 are amorphous, whereas mica and h-BN are layered crystalline materials. Hence, at present, it is only meaningful to compare the mica data with h-BN. Clearly, further studies such as density functional theory, molecular dynamics simulations, and high resolution transmission electron microscopy are essential to elucidate the BD mechanism at the atomic scale.

Conclusion

We have performed localized electrical breakdown measurements on 2D muscovite mica flakes of ~ 2 to 15 nm thickness by CAFM. This is the first dedicated study of mica breakdown since the seminal work of Davidson and Yoffe^{22,23} on thick (> 20 nm) mica sheets. For CAFM studies, we have found that there are three important issues to address to obtain robust BD data. First, the BD locations must be spaced sufficiently far apart (> 1 μm) to ensure that there is no interference between measurements. Second, the current compliance must be set to a very

low value (< 1 nA) to ensure severe damage does not occur to the sample in a BD event. Finally, swelling of the mica occurs once a current begins to flow. The origins of the swelling are not understood at present (we surmise it could be due to the field driven diffusion/ electro-thermo migration of potassium ions) but from an experimental viewpoint, the BD data should be treated with caution for locations where excessive swelling is observed.

We find that 2D muscovite mica has a high electrical breakdown strength (12 MV/cm or more) and low leakage current, comparable to 2D h-BN of similar thickness. However, a significant difference compared to h-BN and conventional thin film dielectrics is the very small current compliance necessary to avoid catastrophic damage in a BD event, even for very thin (2–3ML) flakes. The resulting BD I - V data always appears very abrupt and no progressive BD process can be definitively observed, although a measurable current flow is required prior to initiation of the BD event (presumably due to the generation of defects). No atomistic understanding is available at present for mica BD and we suggest a general reason for the marked differences between mica and h-BN to arise from the poor thermal conductivity (two orders of magnitude lower than h-BN) of mica. As power cannot be effectively dissipated, the temperature rise at the BD location can be rapid and large, leading to thermally induced damage even at very low currents.

Methods

We use V1 grade muscovite natural mica (50 mm \times 75 mm \times 0.15 mm substrates) from Ted Pella, Inc. and Fluorophlogopite synthetic mica (20 mm \times 10 mm \times 0.2 mm substrates) from Changchun City Taiyuan Fluorophlogopite Co. Ltd. for preparing natural mica and synthetic mica flakes, respectively. Gold assisted mechanical exfoliation of mica is used (Supplementary Fig. S1) with the mechanical exfoliation of the bulk mica performed using a polyurethane gel roller of diameter 20 mm (EX-230-AS, EXSEAL, Co, Ltd, Mino, Japan)²⁷. The resulting 2D mica layers attached to the roller are immediately transferred onto a freshly deposited gold surface under clean room conditions. The gold film is 20 nm thick with a 2 nm titanium adhesion layer and is deposited on a silicon substrate by electron beam evaporation (Denton Explorer).

The resulting flakes on the gold surface are first imaged optically and then imaged using an Atomic Force Microscope (AFM). The AFM system used (JPK NanoWizard 3) is first operated in tapping mode (using Tap190-G, $k_c = 48$ N/m cantilevers from Budget Sensors, with k_c being the cantilever stiffness) to obtain high resolution images of the flakes. Once suitable flakes are identified, CAFM is used to perform localized BD on the flakes by RVS. A Keithley 4200 Semiconductor Characterization System is used for RVS to force voltage onto the tip and measure the current passing through the tip (Fig. 2). The gold substrate is grounded. We find that to avoid catastrophic electrical damage of the mica, the Keithley 4200 must operate at a low current measurement range (1nA) and very low current compliance (typically < 0.1 nA).

Two types of tips are used for CAFM, namely Platinum Iridium wire cantilevers (Rocky Mountain Nanotechnology 25PtIr300B, $k_c = 22$ N/m) and conducting diamond cantilevers (Budget Sensors CDT-FMR, $k_c = 6.2$ N/m). The tip resistance is constantly checked during CAFM measurements by moving off a mica flake and measuring the I - V on the nearby gold surface. A representative I - V taken on gold is shown in Supplementary Fig. 6. This check is important for CAFM on insulating samples such as mica to ensure the tip apex maintains low resistance electrical characteristics and is not damaged or contaminated. CAFM measurements are taken in ambient conditions under flowing nitrogen to decrease the relative humidity to $\sim 20\%$ and only positive bias is applied to the tip; both arrangements are to mitigate effects of local anodic oxidation at the tip^{47,48}. Finally, it is worth noting that the total measurement time for each point selected takes less than a minute and hence, with the cantilevers used, the lateral drift of the tip location is not significant for the measurements presented⁴⁹.

Data availability

The data that support the findings of this study are available from the corresponding author upon reasonable request.

Received: 8 July 2022; Accepted: 9 August 2022

Published online: 18 August 2022

References

1. Taur, Y. & Ning, T. H. *Fundamentals of Modern VLSI Devices* (Cambridge University Press, USA, 2021).
2. Gao, F., Yang, H. & Hu, P. Interfacial engineering for fabricating high-performance field-effect transistors based on 2D materials. *Small Methods* **2**, 1700384. <https://doi.org/10.1002/smt.201700384> (2018).
3. Lemme, M. C., Akinwande, D., Huyghebaert, C. & Stampfer, C. 2D materials for future heterogeneous electronics. *Nat. Commun.* <https://doi.org/10.1038/s41467-022-29001-4> (2022).
4. Knobloch, T. *et al.* The performance limits of hexagonal boron nitride as an insulator for scaled CMOS devices based on two-dimensional materials. *Nat. Electron.* **4**, 98–108. <https://doi.org/10.1038/s41928-020-00529-x> (2021).
5. Illarionov, Y. Y. *et al.* Insulators for 2D nanoelectronics: The gap to bridge. *Nat. Commun.* **11**, 3385. <https://doi.org/10.1038/s41467-020-16640-8> (2020).
6. Castellanos-Gomez, A. *et al.* Atomically thin mica flakes and their application as ultrathin insulating substrates for graphene. *Small* **7**, 2491–2497. <https://doi.org/10.1002/sml.201100733> (2011).
7. de Poel, W. *et al.* Muscovite mica: Flatter than a pancake. *Surf. Sci.* **619**, 19–24. <https://doi.org/10.1016/j.susc.2013.10.008> (2014).
8. Kalita, J. M. & Wary, G. Estimation of band gap of muscovite mineral using thermoluminescence (TL) analysis. *Phys. B* **485**, 53–59. <https://doi.org/10.1016/j.physb.2016.01.009> (2016).
9. Rosenholtz, J. L. & Smith, D. T. The dielectric constant of mineral powders. *Am. Miner.* **21**, 115–120 (1936).
10. Barlow, S. G. & Manning, D. A. C. Influence of time and temperature on reactions and transformations of muscovite mica. *Br. Ceram. Trans.* **98**, 122–126. <https://doi.org/10.1179/096797899680327> (1999).
11. Wang, S. *et al.* 2D Bi₂Se₃ van der Waals epitaxy on mica for optoelectronics applications. *Nanomaterials (Basel)* **10**, 1653. <https://doi.org/10.3390/nano10091653> (2020).

12. Zhang, X., He, Y., Li, R., Dong, H. & Hu, W. 2D mica crystal as electret in organic field-effect transistors for multistate memory. *Adv. Mater.* **28**, 3755–3760. <https://doi.org/10.1002/adma.201506356> (2016).
13. Zou, X. *et al.* Damage-free mica/MoS₂ interface for high-performance multilayer MoS₂ field-effect transistors. *Nanotechnology* **30**, 345204. <https://doi.org/10.1088/1361-6528/ab1ff3> (2019).
14. Lee, C.-Y. & Chang, C.-W. Dielectric constant enhancement with low dielectric loss growth in graphene oxide/mica/polypropylene composites. *J. Compos. Sci.* <https://doi.org/10.3390/jcs5020052> (2021).
15. Liu, Y. *et al.* Epitaxial growth of ternary topological insulator Bi₂Te₂Se 2D crystals on mica. *Small* **13**, 1603572 (2017).
16. Hu, H. *et al.* Flexible and electrically tunable plasmons in graphene-mica heterostructures. *Adv. Sci.* **5**, 1800175. <https://doi.org/10.1002/advs.201800175> (2018).
17. Low, C. G., Zhang, Q., Hao, Y. & Ruoff, R. S. Graphene field effect transistors with mica as gate dielectric layers. *Small* **10**, 4213–4218 (2014).
18. He, Y. *et al.* Mica, a potential two-dimensional-crystal gate insulator for organic field-effect transistors. *Adv. Mater.* **23**, 5502–5507. <https://doi.org/10.1002/adma.201103592> (2011).
19. Low, C. G. & Zhang, Q. Ultra-thin and flat mica as gate dielectric layers. *Small* **8**, 2178–2183 (2012).
20. Bitla, Y. & Chu, Y.-H. MICATronics: A new platform for flexible X-tronics. *FlatChem* **3**, 26–42. <https://doi.org/10.1016/j.flatc.2017.06.003> (2017).
21. Zhang, R. *et al.* Realization of a non-markov chain in a single 2D mineral RRAM. *Sci. Bull.* **66**, 1634–1640. <https://doi.org/10.1016/j.scib.2021.04.025> (2021).
22. Davidson, A. T. & Yoffe, A. D. Dielectric breakdown in thin mica crystals. *Nature* **206**, 1247–1248. <https://doi.org/10.1038/2061247a0> (1965).
23. Davidson, A. T. & Yoffe, A. D. Hopping electrical conduction and thermal breakdown in natural and synthetic mica. *Phys. Status Solidi B* **30**, 741–754. <https://doi.org/10.1002/pssb.19680300234> (1968).
24. Liang, J.-J. & Hawthorne, F. C. Rietveld refinement of micaceous materials; muscovite-2M 1, a comparison with single-crystal structure refinement. *Can. Mineral.* **34**, 115–122 (1996).
25. Frisenda, R., Niu, Y., Gant, P., Muñoz, M. & Castellanos-Gomez, A. Naturally occurring van der Waals materials. *npj 2D Mater. Appl.* **4**, 1–13. <https://doi.org/10.1038/s41699-020-00172-2> (2020).
26. Jia, F. & Song, S. Preparation of monolayer muscovite through exfoliation of natural muscovite. *RSC Adv.* **5**, 52882–52887. <https://doi.org/10.1039/c5ra07749d> (2015).
27. Islam, M. R. & Tomitori, M. Evaluation of the discrete thickness of exfoliated artificially synthesized mica nanosheets on silicon substrates: Toward characterization of the tunneling current through the nanosheets. *Appl. Surf. Sci.* **532**, 147388. <https://doi.org/10.1016/j.apsusc.2020.147388> (2020).
28. Desai, S. B. *et al.* Gold-mediated exfoliation of ultralarge optoelectronically-perfect monolayers. *Adv. Mater.* **28**, 4053–4058. <https://doi.org/10.1002/adma.201506171> (2016).
29. Heyl, M. *et al.* Thermally activated gold-mediated transition metal dichalcogenide exfoliation and a unique gold-mediated transfer. *Phys. Status Solidi (RRL) Rapid Res. Lett.* **14**, 200–408 (2020).
30. Velicky, M. *et al.* Mechanism of gold-assisted exfoliation of centimeter-sized transition-metal dichalcogenide monolayers. *ACS Nano* **12**, 10463–10472. <https://doi.org/10.1021/acsnano.8b06101> (2018).
31. Ranjan, A. *et al.* Dielectric breakdown in single-crystal hexagonal boron nitride. *ACS Appl. Electron. Mater.* **3**, 3547–3554. <https://doi.org/10.1021/acsaem.1c00469> (2021).
32. Jiang, L. *et al.* Dielectric breakdown in chemical vapor deposited hexagonal boron nitride. *ACS Appl. Mater. Interfaces* **9**, 39758–39770. <https://doi.org/10.1021/acsaem.7b10948> (2017).
33. Lantz, M. A., O'Shea, S. J. & Welland, M. E. Simultaneous force and conduction measurements in atomic force microscopy. *Phys. Rev. B* **56**, 15345–15352. <https://doi.org/10.1103/PhysRevB.56.15345> (1997).
34. Robertson, J. High dielectric constant oxides. *Eur. Phys. J. Appl. Phys.* **28**, 265–291. <https://doi.org/10.1051/epjap:2004206> (2004).
35. Britnell, L. *et al.* Electron tunneling through ultrathin boron nitride crystalline barriers. *Nano Lett.* **12**, 1707–1710. <https://doi.org/10.1021/nl3002205> (2012).
36. McPherson, J. W. Increases in Lorentz factor with dielectric thickness. *World J. Condens. Matter Phys.* **06**, 152–168. <https://doi.org/10.4236/wjcmp.2016.62018> (2016).
37. McPherson, J., Kim, J., Shanware, A., Mogul, H. & Rodriguez, J. In *Digest. International Electron Devices Meeting* 633–636 (IEEE).
38. Kim, S. S. *et al.* Tunable bandgap narrowing induced by controlled molecular thickness in 2D mica nanosheets. *Chem. Mater.* **27**, 4222–4228. <https://doi.org/10.1021/cm504802j> (2015).
39. Ranjan, A. *et al.* In *2018 IEEE International Reliability Physics Symposium (IRPS)* 1–6 (IEEE).
40. Hattori, Y., Taniguchi, T., Watanabe, K. & Nagashio, K. Layer-by-layer dielectric breakdown of hexagonal boron nitride. *ACS Nano* **9**, 916–921. <https://doi.org/10.1021/nn506645q> (2015).
41. Ranjan, A., O'Shea, S. J., Bosman, M., Raghavan, N. & Pey, K. L. Localized probing of dielectric breakdown in multilayer hexagonal boron nitride. *ACS Appl. Mater. Interfaces* **12**, 55000–55010. <https://doi.org/10.1021/acsaem.0c17107> (2020).
42. Lombardo, S. *et al.* Dielectric breakdown mechanisms in gate oxides. *J. Appl. Phys.* **98**, 121301. <https://doi.org/10.1063/1.2147714> (2005).
43. Palumbo, F. *et al.* A review on dielectric breakdown in thin dielectrics: Silicon dioxide, high-k, and layered dielectrics. *Adv. Funct. Mater.* **30**, 1900657. <https://doi.org/10.1002/adfm.201900657> (2020).
44. Degraeve, R. *et al.* New insights in the relation between electron trap generation and the statistical properties of oxide breakdown. *IEEE Trans. Electron Devices* **45**, 904–911. <https://doi.org/10.1109/16.662800> (1998).
45. Zhang, K., Feng, Y., Wang, F., Yang, Z. & Wang, J. Two dimensional hexagonal boron nitride (2D-hBN): Synthesis, properties and applications. *J. Mater. Chem. C* **5**, 11992–12022. <https://doi.org/10.1039/c7tc04300g> (2017).
46. Zhu, W., Zheng, G., Cao, S. & He, H. Thermal conductivity of amorphous SiO₂ thin film: A molecular dynamics study. *Sci. Rep.* <https://doi.org/10.1038/s41598-018-28925-6> (2018).
47. Avouris, P., Hertel, T. & Martel, R. Atomic force microscope tip-induced local oxidation of silicon: Kinetics, mechanism, and nanofabrication. *Appl. Phys. Lett.* **71**, 285–287. <https://doi.org/10.1063/1.119521> (1997).
48. Gordon, A. E. Mechanisms of surface anodization produced by scanning probe microscopes. *J. Vacuum Sci. Technol. B Microelectron. Nanometer Struct.* **13**, 2805. <https://doi.org/10.1116/1.588270> (1995).
49. Ranjan, A., Pey, K. L. & O'Shea, S. J. The interplay between drift and electrical measurement in conduction atomic force microscopy. *Rev. Sci. Instrum.* **90**, 073701. <https://doi.org/10.1063/1.5095647> (2019).

Acknowledgements

This work is funded by the SUTD-ZJU IDEA Research Grant, SUTD-ZJU (VP) 201906 and MOE-2019-T2-1-197 (MOE AcRF Tier 2). The first author is grateful to Singapore University of Technology and Design (SUTD) for award of the SUTD Ph.D. Fellowship for his doctoral studies.

Author contributions

A.M. and S.J.O. performed the experiments, analyzed the data, and wrote the manuscript. K.S., N.R, and K.L.P secured project funding, reviewed the experimental design and assisted in manuscript writing. All authors discussed the results and revised the manuscript.

Competing interests

The authors declare no competing interests.

Additional information

Supplementary Information The online version contains supplementary material available at <https://doi.org/10.1038/s41598-022-18320-7>.

Correspondence and requests for materials should be addressed to S.J.O.

Reprints and permissions information is available at www.nature.com/reprints.

Publisher's note Springer Nature remains neutral with regard to jurisdictional claims in published maps and institutional affiliations.



Open Access This article is licensed under a Creative Commons Attribution 4.0 International License, which permits use, sharing, adaptation, distribution and reproduction in any medium or format, as long as you give appropriate credit to the original author(s) and the source, provide a link to the Creative Commons licence, and indicate if changes were made. The images or other third party material in this article are included in the article's Creative Commons licence, unless indicated otherwise in a credit line to the material. If material is not included in the article's Creative Commons licence and your intended use is not permitted by statutory regulation or exceeds the permitted use, you will need to obtain permission directly from the copyright holder. To view a copy of this licence, visit <http://creativecommons.org/licenses/by/4.0/>.

© The Author(s) 2022